Channeling Multikilojoule High-Intensity Laser Beams in an Inhomogeneous Plasma

Propagating a laser beam at relativistic intensities ($>10^{18}$ W/cm^2) through a plasma with a large density scale length is dominated by highly nonlinear interactions including ponderomotive expulsion of electrons,[1] channeling,[2–4] and developing hosing and bifurcation instabilities.[3,4] These effects are important for both fundamental aspects of relativistic laser–plasma interaction physics and applications such as fast ignition in inertial confinement fusion.[5] The central idea of the fast-ignition concept is to first compress a DT ice capsule with a nanosecond, megajoule laser to a high areal density and then use an ultrapowerful short-pulse laser to subsequently ignite the fuel. Since laser light at nonrelativistic intensities propagates in the plasma corona up to only the critical density $n_c = \omega_0^2 m_e \varepsilon_0 / e^2$ (where ω_0 is the laser angular frequency, m_e is the electron mass, ε_0 is the permittivity of free space, and e is the elementary charge), the idea is to use one high-intensity pulse to form a channel through the corona and then inject the ignition pulse into the lower-density plasma column as in an optical waveguide[6] to deposit sufficient energy in the core for ignition. In contrast to the cone-in-shell concept,[7] the channeling concept has the advantage that it uses symmetric implosions and can be readily applied to cryogenic targets. Cryogenic cone-in-shell targets are technically challenging and so far have not been demonstrated. Channeling into dense plasmas relies on the laser intensity to provide sufficient ponderomotive pressure against the outflowing plasma and a laser pulse duration that is long enough to sustain the channel formation. When the laser reaches densities $>n_c$, it may continue to push forward through its ponderomotive pressure ("hole boring") and relativistic transparency. The ponderomotive hole-boring velocity[8,9] is found by balancing the light pressure against the pressure arising from the material stagnating against the head of the channel. For an increasing laser intensity, a higher hole-boring velocity is obtained. For a laser system of fixed energy, increased intensity comes at a price of decreased laser pulse duration or smaller spot size, and the balance between laser intensity and duration must be optimized to provide the longest channel. Channeling experiments with short[10] and long[11] laser pulses were performed, and it was demonstrated both in experiments[12] and simulations[4] that channels have a higher transmission for a trailing pulse compared to an unperturbed plasma.

These experimental observations were carried out using a variety of diagnostics including interferometry,[12] self-emission,[13] and x-ray grid image refractometry.[14] These diagnostics were limited to plasma densities below n_c [here, n_c always refers to infrared (IR) laser light ($\lambda_{IR} = 1.054$ μm)]. The channel region in the vicinity of n_c was unexplored because of the strong refraction of the probe radiation at high plasma densities.

This article describes the observation of laser channeling in millimeter-sized inhomogeneous plasmas by measuring the depth of a channel for laser pulses with peak intensities between $\sim 1 \times 10^{19}$ and $\sim 4 \times 10^{19}$ W/cm^2. The density scale length is comparable to those obtained in high-compression shots with spherical shells on the OMEGA laser. This experiment is relevant to future integrated fast-ignition channeling experiments. To our knowledge, it represents the first measurements of the channel up to n_c in a laser-driven blowoff plasma of this size. The observations reported here were made possible by using a probe with a short wavelength ($\lambda_p = 0.263$ μm) and a sufficiently large solid angle of the collection optics ($\sim f/4$). Measurements of the plasma density in the channel and in the background plasma are presented. The time for the short pulse to reach n_c was measured and compares well to simulation predictions. The experimental results show that for a fixed laser energy, a lower-intensity, longer pulse propagates deeper into a long-scale-length plasma.

The experiments were carried out on the OMEGA EP Laser System.[15] Figure 140.21 shows a schematic of the interaction and probing geometries. Two ultraviolet (UV) ($\lambda_{UV} = 0.351$ μm) laser beams smoothed by distributed phase plates (eighth-order super-Gaussian with 800-μm full width at half maximum)[16] irradiated a 125-μm-thick planar plastic (CH) target to create and heat a blowoff plasma. The UV irradiation delivered 2 kJ of total energy in a 1-ns square pulse. The channeling laser pulse was an IR beam with an energy ranging from 0.75 kJ to 2.6 kJ. An intensity comparison was performed by using 100-ps and 10-ps pulse widths, respectively. The wavefront of the channeling beam was measured and the focal-spot irradiance map was inferred for each shot.[17] Eighty percent
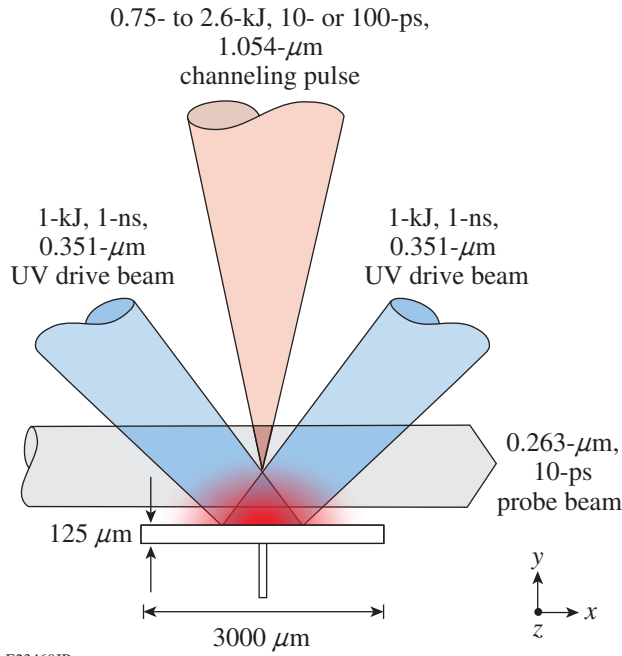
Figure 140.21

Schematic of the experimental setup. A plastic target is illuminated by two UV beams to generate a large expanding plasma plume. Following the UV beams, an IR channeling laser beam is injected into the plume along the density gradient. The interaction is observed by a UV optical probe pulse that is timed to arrive at a specific delay from the start of the channeling pulse.

of the laser energy was contained in a 25-μm spot resulting in vacuum peak intensities of $\sim 1 \times 10^{19}$ and $\sim 4 \times 10^{19}$ W/cm^2 for 2.6-kJ, 100-ps and 1-kJ, 10-ps pulses, respectively. The average laser intensities in the focal spot were about an order of magnitude lower. The focal position of the channeling beam was set to 750 μm from the original target surface, and the corresponding electron plasma density was predicted to be $n_e = 2.5 \times 10^{20}$ cm^{-3}, which is close to $n_c/4$. It has been suggested in Ref. 18 that focusing the laser beam to $n_c/4$ might provide the most-favorable condition for relativistically enhanced propagation. The probe beam[19] was a 10-ps, 0.263-μm laser with 10 mJ of energy. The relative timing between the probe and channeling pulse was measured with an accuracy of better than 20 ps on each shot.

The expanding blowoff plasma was measured by using a new method of optical probing—angular filter refractometry (AFR)[20]—which visualizes gradients in the refractive index n of an object. The refractive index of an unmagnetized, collisionless plasma is given by $n = \sqrt{1 - n_e/n_c}$. Figure 140.22(a) shows an example of such a measurement shortly before the arrival of the channeling beam. The probe light that has passed
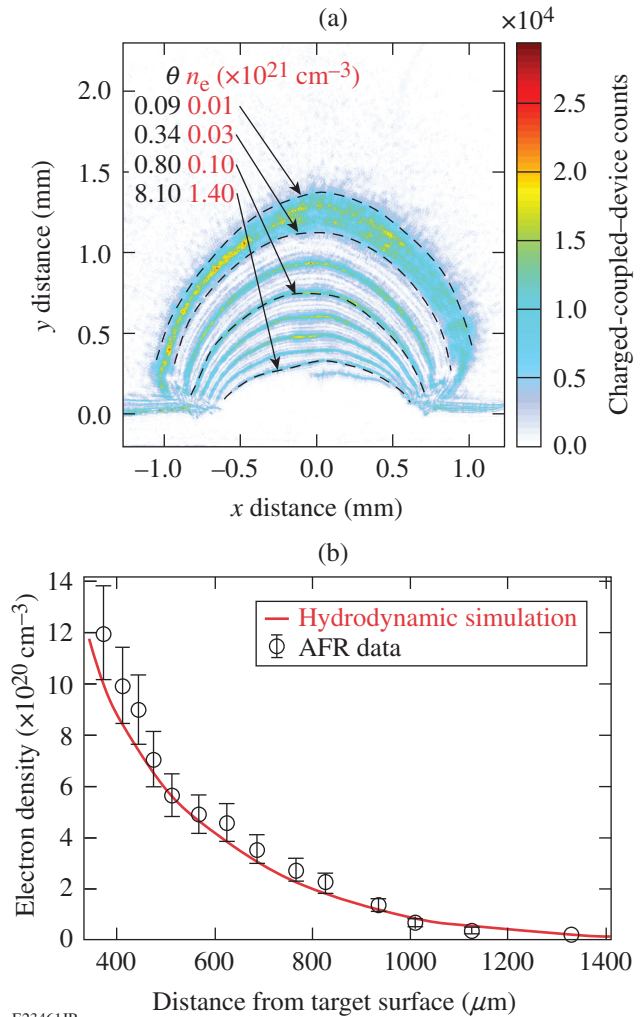

Figure 140.22

(a) Measured optical probe image of the unperturbed long-scale-length plasma (45 ps prior to the arrival of the channeling beam). The original target surface is located at $y = 0$. Contours of the constant refraction angle and associated electron densities are also shown. (b) On-axis lineout of the measured values of the unperturbed electron density (points) versus distance from the target surface. The solid line is a prediction from a 2-D hydrodynamic simulation.

through the plasma is collected and filtered in the focal plane of the collection optics where the spatial locations of probing rays depend on their refraction angle. A bull's-eye–patterned filter with alternating transparent and opaque rings provides isocontours of the refraction angle in the image plane. Using AFR allows one to measure the angular deviation of probe rays while preserving the fine structures in the image, which is a considerable advantage over other methods. AFR, as a refractive method, is capable of probing large plasma volumes, whereas, e.g., interferometric techniques that rely on fringe-shift measurements are severely limited by the large

phase shifts accumulated along the path. The electron plasma density profile shown in Fig. 140.22(b) was inferred from the measured angular deviation θ of probing rays, assuming a hemi-spherical plasma with a varying refractive index. The analysis is described in detail in Ref. 20. The unperturbed on-axis plasma profile in Fig. 140.22(b) is in agreement with two-dimensional (2-D) hydrodynamic simulations with the code *DRACO*.[21] The simulated electron temperature is 1.8 keV. The experimentally determined radial density scale length in the observed region varies from 200 to 320 μm with 250 μm being the average. The last contour in the collection system ($\theta \approx 8.1°$) corresponds to light that is refracted through a peak density above n_c (1.4×10^{21} cm^{-3}).

Figure 140.23 shows measured channels at different probing times for 10-ps and 100-ps laser irradiation. The channel is visualized by the perturbations in the AFR contours. The contours bend as a result of strong density gradients created by the channeling pulse. Figures 140.23(a)–140.23(d) show the results for the 10-ps pulse. At 6 ps the head of the channel reached a position of 450 μm from the original target surface. The electron density at this location corresponds to 0.6 n_c. The channel was observed up to 200 ps after its creation. Later in time, the tip of the channel retreats backward with a velocity of ~3×10^7 cm/s away from the target surface. There is a clear

difference in the channel depth between the 10-ps and 100-ps pulses. The 100-ps pulse [Figs. 140.23(e)–140.23(h)] reach the contour closest to the original target surface, indicating that a density >1.4×10^{21} cm^{-3} has been reached. The 100-ps pulse [as shown in Fig. 140.23(e)] reached, in only 18 ps, about the same depth as the 10-ps pulse. The 100-ps pulse continued to bore through the plasma, reaching overcritical density at 65 ps after the start of the laser beam. The upper contour bands in the lower-density region are smoothly shifted in space, while the contours at higher density inside the channel are highly distorted and obscured. This is likely caused by sharp density modulations at the channel wall that are also observed in particle-in-cell (PIC) simulations.[3,22] Bright fourth-harmonic emission of the channeling beam was measured in the vicinity of the critical surface [Figs. 140.23(e)–140.23(h)] with the 100-ps pulse. Harmonics from the critical-density surface have been observed in experiments with high-intensity laser beams interacting with solid-density plasmas.[23] No harmonic emission was observed with the 10-ps pulse, indicating that it did not reach n_c.

Figure 140.24 shows a radial cross section of the measured density profile in the channel. The density is calculated using an Abel inversion of the phase, which is inferred from the angular refraction in the AFR image. The density profile in the channel
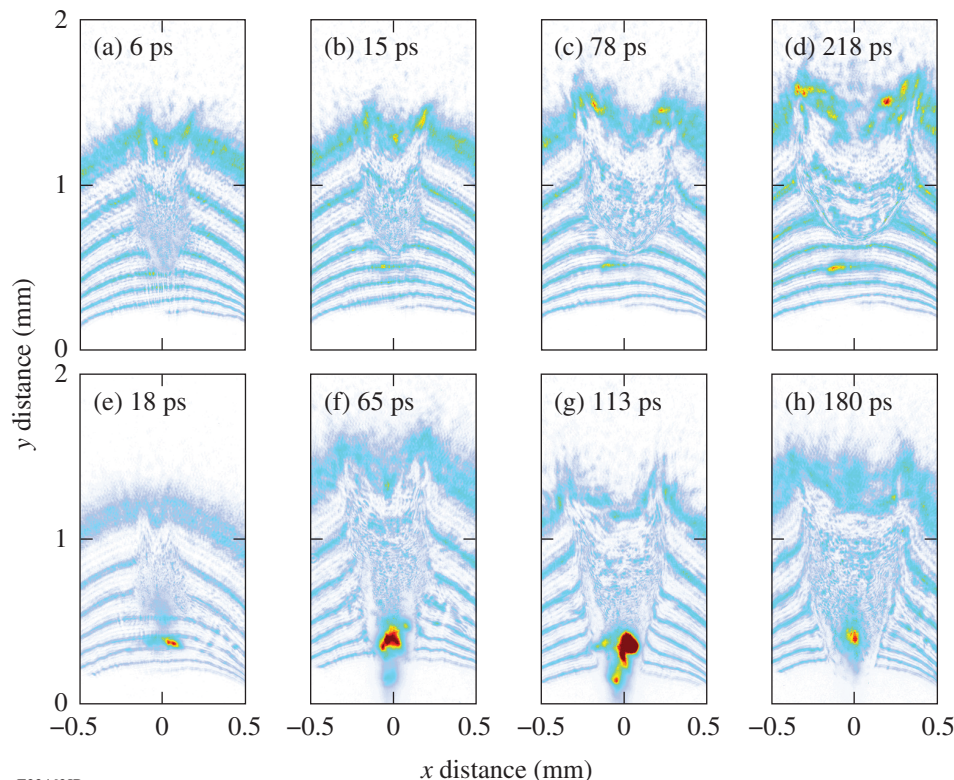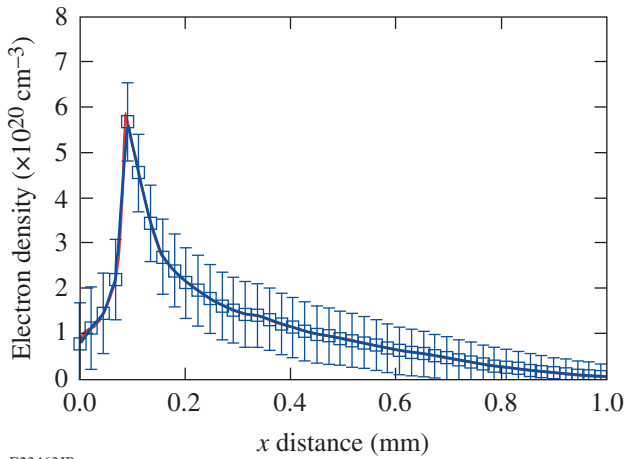

Figure 140.23
Optical probe images for 10-ps and 100-ps channeling laser pulses at various times showing greater penetration depth for the longer pulse. [(a)–(d)] The 10-ps, 125-TW laser pulse never reaches n_c and, therefore, does not produce fourth-harmonic emission. Since the detector integrated over a time much longer than the duration of the probe pulse, the harmonic signal is present even in frames taken before the channel reaches the critical surface in the probe image. Time zero is defined as the start of the short pulse. The background plasma was always the same as the one shown in Fig. 140.22(a). [(e)–(h)] The red spots are caused by fourth-harmonic generation from the 100-ps, 20-TW channeling pulse reaching n_c.

E23462JR

E23463JR

Figure 140.24
Density profile of a channel created by a 100-ps pulse and probed at ~65 ps into the pulse along the x axis at $y = 0.8$ mm. The density on axis is reduced by 65% with respect to the density of the unperturbed plasma at the same location ($n_e = 2 \times 10^{20}$ cm^{-3}). Error bars are calculated from the uncertainty in the measurement of θ.

region takes on a parabolic-like shape bounded on either side by walls with a density higher than the background density. For the specific image shown here, the density in the channel has been reduced from 2×10^{20} cm^{-3} to 7×10^{19} cm^{-3}—a reduction of 65%. The measured density in the channel is about a factor of 2 higher than that predicted by PIC simulations for similar conditions.[3] This image was taken at 65 ps into a 100-ps pulse, so the density may be reduced further. At later times, contours become impossible to identify as the density gradient at the channel wall steepens.

The intensity distribution in the experimental laser focus was not diffraction limited and contained some spatial inhomogeneity,[17] which probably seeded the filamentation instability and self-focusing in the plasma driven by ponderomotive and relativistic effects. Filamentation was predicted by solving the paraxial wave equation with a split-step algorithm, taking into account the ponderomotive and relativistic effects in the refractive index of the plasma and using the measured wavefront map of the channeling beam. The calculated beam inside the plasma was similar in size to the measured channel width. In addition, simultaneous measurements of the strong electrostatic and magnetic fields inside the plasma with proton radiography[24] also concluded the existence of filamentary structures at a location between 0.5 and 1 mm from the initial target surface. Three-dimensional (3-D) hydrodynamic simulations including relativistic corrections and the effect of charge separation have demonstrated that aberrated beams do not channel as effectively

as diffraction-limited beams.[25] Filamentation is sensitive to the power in the laser speckles and, therefore, is expected to be more severe for higher-power pulses. When sufficiently driven, this might cause beam spraying and result in the breakup of the beam so that it cannot reach a higher density. The 100-ps channeling beam had ~4× less power than the 10-ps pulse and is expected to be less affected by filamentation, which might be one of the reasons why this beam propagated deeper into the plasma.

Two- and three-dimensional PIC simulations with large (~500-μm) plasmas studied the propagation and channeling for conditions similar to this experiment.[3,4] The laser power greatly exceeds the power threshold for relativistic self-focusing[26,27] and beam filamentation occurs in the early stage of the simulation. The local intensity increases in the filaments and the resulting transverse ponderomotive force pushes most of the electrons out of the filaments. The resulting space-charge force causes the ions to follow, creating several microchannels that eventually merge together and form a single density channel along the laser-propagation axis. The simulations predict that besides laser hosing, channel bifurcation, and self-correction, the laser front will pile up material at the channel head that will reach densities n_c, even though the surrounding plasma is underdense. The simulations predict that after a short initial period (~ps), when the pulse propagates with a speed close to the linear group velocity, it quickly slows down and, after ~5 ps, approaches the ponderomotive hole-boring velocity.[8,9] The plasma density gradient rapidly steepens in front of the pulse and the laser light essentially interacts most of the time with steep overcritical plasma.[3,4]

The channel propagation velocity can be obtained from the experiment. The depth of the channel is found by measuring the distance from the original target surface to the closest point of perturbed contours in the probe image. A channel progression velocity of >3±1 μm/ps was obtained from the data. The Mach angle gives another measure of the velocity of the supersonic advancing front in the gas. The velocity of the front of the channel is found by measuring the angle of the wake left behind by the channel. The Mach angle relates the front Mach number M to the angle θ_m by $\sin(\theta_m) = 1/M$. The Mach angle is measured to be ~8° [in Fig. 140.23(f)], which gives a channel head Mach number of $M \sim 7$ and a velocity of 2 μm/ps, slightly lower than from the depth measurement.

The measured channel progression velocity is in agreement with PIC simulations, showing that it approaches the hole-boring velocity, given by

$$v_h = c\sqrt{Z(n_c/n_e)(m_e/M_i)(2-\eta_a)I_{18}\lambda_\mu^2/2.74} \qquad (1)$$

for normal incidence light.[9] Here c is the speed of light, Z is the average charge state of the plasma, M_i is the ion mass, η_a is the laser absorption fraction, I_{18} is the laser intensity in units of 10^{18} W/cm^2, and λ_μ is the laser wavelength in units of μm. The hole-boring velocity decreases with $\sqrt{1/n_e}$ when the pulse propagates deeper into the plasma, forcing more material to pile up. For an average intensity of $I = 10^{18}$ W/cm^2, fully ionized plastic, $\eta_a = 1$, and n_e/n_c between 1 and 2, v_h is estimated with 3.2 μm/ps and 2.2 μm/ps, respectively, which is consistent with the measurement.

The 3-D simulations provide scalings for the time T_c that is required for the channel head to reach the position of n_c and the required laser energy E_c, which are given by T_c (ps) $= 1.5 \times 10^2\,I_{18}^{-0.64}$ and E_c (kJ) $= 0.85\,I_{18}^{0.32}$ (Ref. 4). The estimated times and energies are between ~35 ps, 1.9 kJ and ~150 ps, 0.85 kJ for 10^{19} W/cm^2 and 10^{18} W/cm^2, respectively, in rough agreement with the experimental values. This scaling also demonstrates that the 10-ps pulse is too short and does not have enough energy to reach n_c. The time it takes for the pulse to bore through one scale-length distance is 250 μm/(3 μm/ps) ~ 80 ps. This indicates that the channeling process is driven primarily by the ponderomotive force as predicted by the 2-D and 3-D PIC simulations.[3,4]

ACKNOWLEDGMENT

REFERENCES

1. K.-C. Tzeng and W. B. Mori, Phys. Rev. Lett. **81**, 104 (1998).

2. A. Pukhov and J. Meyer-ter-Vehn, Phys. Rev. Lett. **76**, 3975 (1996).

3. G. Li, R. Yan *et al.*, Phys. Rev. Lett. **100**, 125002 (2008).

4. G. Li *et al.*, Phys. Plasmas **18**, 042703 (2011).

5. M. Tabak *et al.*, Phys. Plasmas **1**, 1626 (1994).

6. C. G. Durfee and H. M. Milchberg, Phys. Rev. Lett. **71**, 2409 (1993).

7. R. Kodama *et al.*, Nature **412**, 798 (2001).

8. W. L. Kruer, E. J. Valeo, and K. G. Estabrook, Phys. Rev. Lett. **35**, 1076 (1975).

9. S. C. Wilks *et al.*, Phys. Rev. Lett. **69**, 1383 (1992).

10. K. A. Tanaka *et al.*, Plasma Phys. Control. Fusion **46**, B41 (2004).

11. P. E. Young *et al.*, Phys. Rev. Lett. **75**, 1082 (1995).

12. J. Fuchs *et al.*, Phys. Rev. Lett. **105**, 225001 (2010).

13. M. Borghesi *et al.*, Phys. Rev. Lett. **78**, 879 (1997).

14. K. Takahashi *et al.*, Phys. Rev. Lett. **84**, 2405 (2000).

15. L. J. Waxer, D. N. Maywar, J. H. Kelly, T. J. Kessler, B. E. Kruschwitz, S. J. Loucks, R. L. McCrory, D. D. Meyerhofer, S. F. B. Morse, C. Stoeckl, and J. D. Zuegel, Opt. Photonics News **16**, 30 (2005).

16. T. J. Kessler, Y. Lin, J. J. Armstrong, and B. Velazquez, in *Laser Coherence Control: Technology and Applications*, edited by H. T. Powell and T. J. Kessler (SPIE, Bellingham, WA, 1993), Vol. 1870, pp. 95–104.

17. B. E. Kruschwitz, S. W. Bahk, J. Bromage, M. D. Moore, and D. Irwin, Opt. Express **20**, 20,874 (2012).

18. T. Matsuoka *et al.*, Plasma Phys. Control. Fusion **50**, 105011 (2008).

19. D. H. Froula, R. Boni, M. Bedzyk, R. S. Craxton, F. Ehrne, S. Ivancic, R. Jungquist, M. J. Shoup, W. Theobald, D. Weiner, N. L. Kugland, and M. C. Rushford, Rev. Sci. Instrum. **83**, 10E523 (2012).

20. D. Haberberger, S. Ivancic, S. X. Hu, R. Boni, M. Barczys, R. S. Craxton, and D. H. Froula, Phys. Plasmas **21**, 056304 (2014).

21. P. B. Radha, T. J. B. Collins, J. A. Delettrez, Y. Elbaz, R. Epstein, V. Yu. Glebov, V. N. Goncharov, R. L. Keck, J. P. Knauer, J. A. Marozas, F. J. Marshall, R. L. McCrory, P. W. McKenty, D. D. Meyerhofer, S. P. Regan, T. C. Sangster, W. Seka, D. Shvarts, S. Skupsky, Y. Srebro, and C. Stoeckl, Phys. Plasmas **12**, 056307 (2005).

22. L. Willingale, P. M. Nilson, A. G. R. Thomas, J. Cobble, R. S. Craxton, A. Maksimchuk, P. A. Norreys, T. C. Sangster, R. H. H. Scott, C. Stoeckl, C. Zulick, and K. Krushelnick, Phys. Rev. Lett. **106**, 105002 (2011).

23. J. Zhang *et al.*, Phys. Rev. A **54**, 1597 (1996).

24. Y. Uematsu, S. Ivancic, T. Iwawaki, H. Habara, A. L. Lei, W. Theobald, and K. A. Tanaka, Rev. Sci. Instrum. **85**, 11E612 (2014).

25. D. E. Hinkel *et al.*, Phys. Plasmas **5**, 1887 (1998).

26. C. Max, J. Arons, and A. B. Langdon, Phys. Rev. Lett. **33**, 209 (1974).

27. B. I. Cohen and C. E. Max, Phys. Fluids **22**, 1115 (1979).